Materials Advances

ROYAL SOCIETY OF CHEMISTRY

PAPER

View Article Online
View Journal | View Issue

Cite this: *Mater. Adv.*, 2025, **6**, 8063

Dual molecular interaction-triggered stable proton conductive channels in heteroatom-embedded covalent organic frameworks

Vellaichamy Joseph, [a] Keiichiro Maegawa, [a] Hassan Alipour, [a] Marek J. Potrzebowski, [b] Krzysztof Łyczko [c] and Atsushi Nagai *[a]

Received 8th July 2025,
Accepted 22nd September 2025

DOI: 10.1039/d5ma00722d

rsc.li/materials-advances

Two covalent organic frameworks (COFs), TZ-COF and TP-COF, were synthesized from triformylphloroglucinol (Tp) building blocks by varying the heteroatom-embedded linkers with either pyridine or triazine rings, and then characterized systematically. Pyridine scaffolds present in TP-COF act as an active site for binding an external proton source (*i.e.*, H_3PO_4; PA) *via* hydrogen bonding interaction to accommodate them within the pores of the COF skeleton. The density functional theory calculation revealed a synergistic ionic hydrogen bonding interaction between PA and pyridinic nitrogen/carbonyl oxygen. This interaction leads to a dense amount of phosphoric acid tightly bound along the 1D pore channels in PA@TP-COF (PA-doped TP-COF), as compared to PA@TZ-COF (PA-doped TZ-COF), which has hydrogen bonding between PA and carbonyl oxygen groups. As a result, the proton conductivity of PA@TP-COF is enhanced up to 7.9×10^{-3} S cm^{-1} under anhydrous conditions at 140 °C. Furthermore, the proton conductivity increases to 1.2×10^{-2} S cm^{-1} under humidified conditions (80 °C and 95% RH), and its initial proton conductivity is complemented to 1.8×10^{-2} S cm^{-1} after 96 h under prolonged exposure to the same temperature and humidity. The confined hydrated hydrogen bonds account for the action of the newly formed proton pathway in the 1D channels.

1. Introduction

Proton conduction is a ubiquitous phenomenon responsible for the function of energy conversion and storage devices like fuel cells and flow batteries.[1–3] The convenient utilization of hydrogen energy into electrical energy in proton exchange membrane (PEM) fuel cells has received immense attention in the last few decades. The core component of PEM fuel cells is the proton conducting material.[4] Many polymers, including Nafion and Flemion, were investigated to demonstrate high proton conduction. However, limited operating temperature (0–80 °C), poor stability, and high cost of synthesis restrict their further development. Additionally, the amorphous nature of such polymers leads to difficulty in controlling the pore environment and precise molecular structure, which hampers further understanding of the proton conducting mechanism.[5–7] Alternatively, crystalline polymers with a precise molecular structure exhibiting proton conductivity under harsh conditions (high temperature and low humidity) are indispensable to overcome the constraints of conventional polymers.

Covalent organic frameworks (COFs) are a distinct class of organic crystalline porous materials exhibiting excellent material characteristics, such as high surface area, tunable pore size, structural periodicity, and high thermal and chemical stability.[8–12] They are fashioned through strong covalent bond knitting. Pre-designed organic building blocks and tailorable linkers could afford attractive properties in COFs, which make them valuable in a wide range of applications such as gas storage, catalysis, sensors, light harvesting, and proton conductors in fuel cells.[13–18] Artificial generation of ion channels that facilitate the proton transfer has garnered significant interest for accelerating proton conduction and promoting power output. COFs provide such 1D channels that enable smooth proton migration. For instance, COFs constructed with building blocks containing functional groups having reversibly dissociable protons exhibit intrinsic proton conduction.[19–21] However, the magnitude of proton conduction in such a system is inferior to achieving practical application in proton exchange membranes. On the other hand, external proton sources such as imidazole, phosphoric acid, phytic acid, *etc.*, are doped into the pore channels of the COF to secure a reliable and sufficient

[a] *Next-Generation Energy Systems group, Centre of Excellence ENSEMBLE3 sp. z o.o., Wólczyńska 133, Warsaw, 01-919, Poland. E-mail: atsushi.nagai@ensemble3.eu*
[b] *Center of Molecular and Macromolecular Studies, Polish Academy of Sciences, Sienkiewicza 112, Lodz, 90-363, Poland*
[c] *Institute of Nuclear Chemistry and Technology, Dorodna 16, Warsaw, 03-195, Poland*

magnitude of proton conduction.[22–25] In particular, the effective hydrogen bonding interaction between the external proton source and the heteroatom present in the COF skeleton results in confinement of such proton carriers, which provides enhanced proton conductivity and prevents acid leakage owing to tightly bound phosphoric acid.[26,27] Here, proton conduction follows either the Grotthuss (<0.4 eV) or vehicular mechanism (>0.4 eV) depending on the energy of activation.[28–30] In water-mediated proton conduction, proton migration involving the Grotthuss mechanism *via* the hydrogen bond network is dominant, which bestows collective proton migration. Thus, confinement of proton carriers/water molecules within the pore channels would trigger proton conductivity to a higher magnitude.[31,32] In addition, abundant nitrogen sites in the pore wall of the COF skeleton offer numerous hydrogen-bonding sites, allowing multiple coordination with proton sources, providing a dense proton source within the pore channel and thereby delivering enhanced proton conductivity.[33–36] Here, we report the synthesis and systematic characterization of two COFs (TZ-COF and TP-COF) containing triazine or pyridine groups in their single pore wall. Both COFs show excellent thermal stability and inherent porosity with high crystallinity. Since the intrinsic proton-conducting groups are absent on both COFs, the as-synthesized COFs showed no assessable proton conductivity. Furthermore, the high thermal stability and porosity of these COFs allowed them to be doped with an external proton source (phosphoric acid; PA) and extended the possibility to accommodate them within the pore channels. Notably, maximum proton conductivity of 7.9×10^{-3} S cm^{-1} was registered for phosphoric acid-doped TP-COF (PA@TP-COF) at 140 °C under anhydrous conditions. Furthermore, proton conductivity was boosted to 1.2×10^{-2} S cm^{-1} under humidified conditions (80 °C, 95% RH).

2. Materials and methods

Synthesis

The synthetic route for both COFs is depicted in Scheme 1. Triformylphloroglucinol (Tp, 1 eq.), 4,4′,4″-(1,3,5-triazine-2,4,6-triyl)trianiline, (TZ-A) or 5,5′,5″-(benzene-1,3,5-triyl)tris(pyridin-2-amine), (TP-A) (1 eq.), and a mixture of solvent (DMAc : *o*-DCB : AcOH(6 M), 3 : 1 : 0.4, v/v/v) were treated in a reaction tube. Following 10 minutes of sonication, the reaction mixture was flash-frozen at 77 K and degassed *via* three freeze–pump–thaw cycles. The reaction tube was sealed off and heated at 120 °C for 72 h. After cooling to RT, the collected yellow precipitate was filtered and washed with DMAc several times, followed by solvent exchange with acetone 6–7 times and dried under vacuum to get the corresponding COFs.

3. Results and discussion

FTIR spectra verify the complete consumption of precursors and the successful formation of targeted COFs. The transformation of the precursors into desired COFs is evidenced by the disappearance of the aldehyde stretching band ~1650 cm^{-1} in Tp and the emergence of a new band between 1614 and 1624 cm^{-1}, corresponding to the C=O bond (keto group). The stretching band for C=C (adjacent to C=O) appears at ~1570 cm^{-1} and the appearance of the C–N stretching band at ~1280 cm^{-1} confirms the successful synthesis of COFs (Fig. 1a). The retention of the band between ~1509 and 1489 cm^{-1} indicates the C=N group from the triazine and pyridine moiety. The band between ~1434 and 1454 cm^{-1} corresponds to the C=C bond in the aromatic phenyl/pyridine linker. After PA doping, an additional band at ~990 cm^{-1} indicates the presence of a P=O group, and the band at ~480–490 cm^{-1}

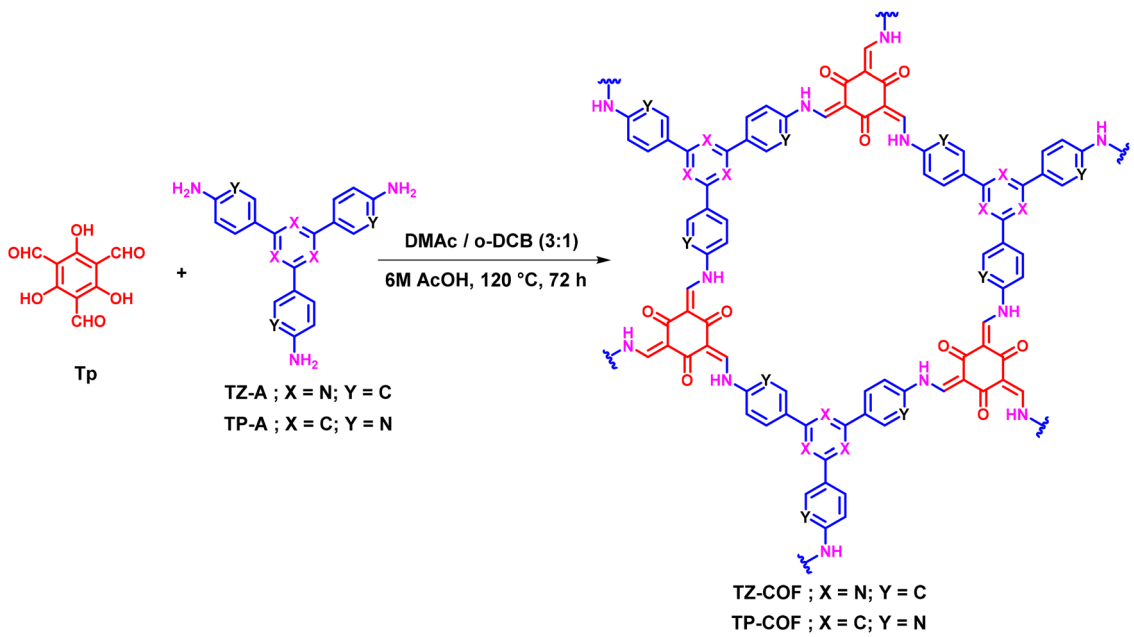

Scheme 1 Synthetic route for covalent organic frameworks (TZ-COF and TP-COF).

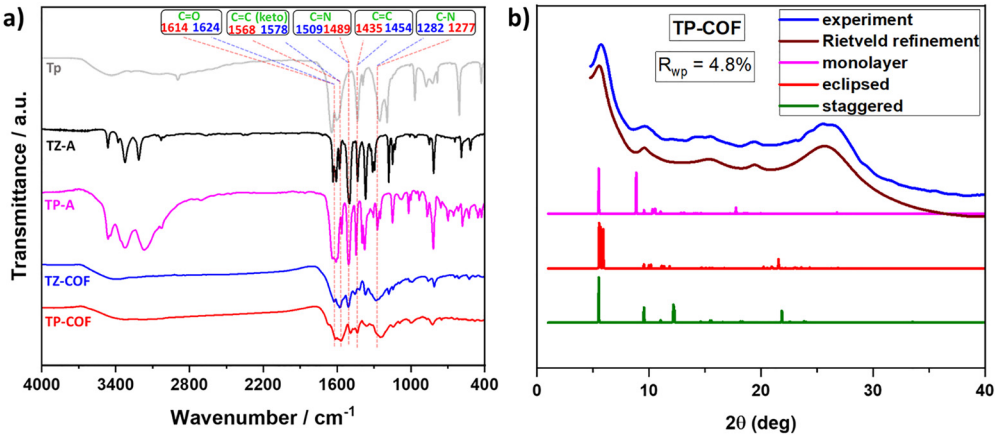

Fig. 1 (a) FTIR spectra of the COFs compared with the precursors. (b) PXRD of TP-COF compared with simulated results.

shows the presence of $H_2PO_4^-$ ions, which confirms the doping of phosphoric acid into the COFs (Fig. S1). The remaining bands remain intact before and after PA doping, which suggests the stability of the COFs in phosphoric acid.

Powder X-ray diffraction (PXRD) analysis confirms the crystallinity of the synthesized COFs, with a high intensity peak appearing at 5.7°, attributed to the (100) crystal plane lattice (Fig. 1b and Fig. S2 and S3). TZ-COF displayed peaks at 5.7, 9.8, 14.9, 18.4, and 26.7° while TP-COF showed peaks at 5.7, 9.7, 15.6, 19.4, and 25.7°. The crystallinity of these COFs could be attributed to keto–enol tautomerization, which restrains long-range ordered stacking.[37] The simulated PXRD pattern of the eclipsed stacking model matched well with the experimental PXRD pattern of the corresponding COFs. The observed broad peak and deviation of the simulated pattern from the experimental PXRD pattern could be ascribed to the smaller particle size of the COFs. The thermal stability of the COFs was assessed using thermogravimetric analysis (TGA) under a nitrogen atmosphere at a heating rate of 10 °C min^{-1}. A decomposition temperature above 280 °C is observed for both COFs corresponding to 5% weight loss, which indicates the thermal robustness of the COF skeleton (Fig. S5). Further, PA@TZ-COF and PA@TP-COF exhibited a slight decline in weight up to 160 °C, corresponding to evaporation/removal of phosphoric acid. The high thermal stability of the PA-doped COFs demonstrates their potential for high temperature proton conduction, which is corroborated by the unaltered FTIR spectra of the PA-doped COFs.

The porosity of the COFs was estimated by N_2 adsorption/desorption measurements at 77 K. Both COFs demonstrated a characteristic type-IV isotherm, marked by a sharp adsorption uptake at low pressure, signifying their mesoporous nature (Fig. S6). The surface area of TZ-COF and TP-COF, calculated using the Brunauer–Emmett–Teller (BET) model, is 608 and 430 m^2 g^{-1}, respectively. The nanopore size distribution centered at 2.7 nm for TZ-COF and 2.2 nm for TP-COF, respectively (Fig. S7), which suggests that phosphoric acid molecules (PA diameter = 0.373 nm)[38] can be confined within their pores. Furthermore, the BET surface area of PA@TZ-COF and PA@TP-COF is reduced to 56 and 11 m^2 g^{-1}, respectively, which confirms the successful impregnation of phosphoric acid into the pores (Fig. S8).

The solid-state ^{13}C NMR (CP-MAS spectra) of TZ-COF and TP-COF revealed the formation of the desired products (Fig. S9). The peak at ~183 ppm is attributed to the carbonyl carbon (keto group) present in both COFs. The apparent peak at ~169 ppm indicates the triazine carbon in TZ-COF.[36] The morphology of the COFs was investigated by scanning electron microscopy (SEM) measurements. The SEM images reveal that the COFs possess a fibrous morphology (Fig. S10). Transmission electron microscopy (TEM) images of both COFs indicate that they possess a layered structural morphology with a porous structure (Fig. 2a and b).

The XPS analysis was carried out for both COFs to examine their interaction and chemical composition (Fig. 2c and d). The binding energy of N 1s in TZ-COF indicates the existence of two types of nitrogen, one peak at 399.0 eV corresponds to the triazine nitrogen (–C═N) and another peak at 400.6 eV indicates the free secondary amine (–NH). On the other hand, the N 1s peak for TP-COF at 399.2 eV corresponds to the pyridinic nitrogen, and the peak at 400.4 eV represents a free secondary amine (–NH).

The proton conductivity of the COFs was evaluated by alternative current (AC) electrochemical impedance spectroscopy measurements. Since both COFs do not have intrinsic dissociating protons (like sulfonic acid) in their skeleton, the as synthesized COFs showed no perceivable proton conduction under both anhydrous and humidified conditions (Fig. S12 and S13). Furthermore, the proton conductivity of H_3PO_4-doped TZ-COF and TP-COF was examined under anhydrous conditions (Fig. 3a and Fig. S14). H_3PO_4-doped TZ-COF and TP-COF were denoted as PA@TZ-COF and PA@TP-COF, respectively. The proton conductivity of PA@TZ-COF and PA@TP-COF was progressively increased with respect to temperature rising from 60 to 140 °C. In particular, maximum proton conductivity of 7.9×10^{-3} S cm^{-1} was recorded for PA@TP-COF at 140 °C under anhydrous conditions, while PA@TZ-COF showed 2.9×10^{-4} S cm^{-1} under the same measurement conditions.

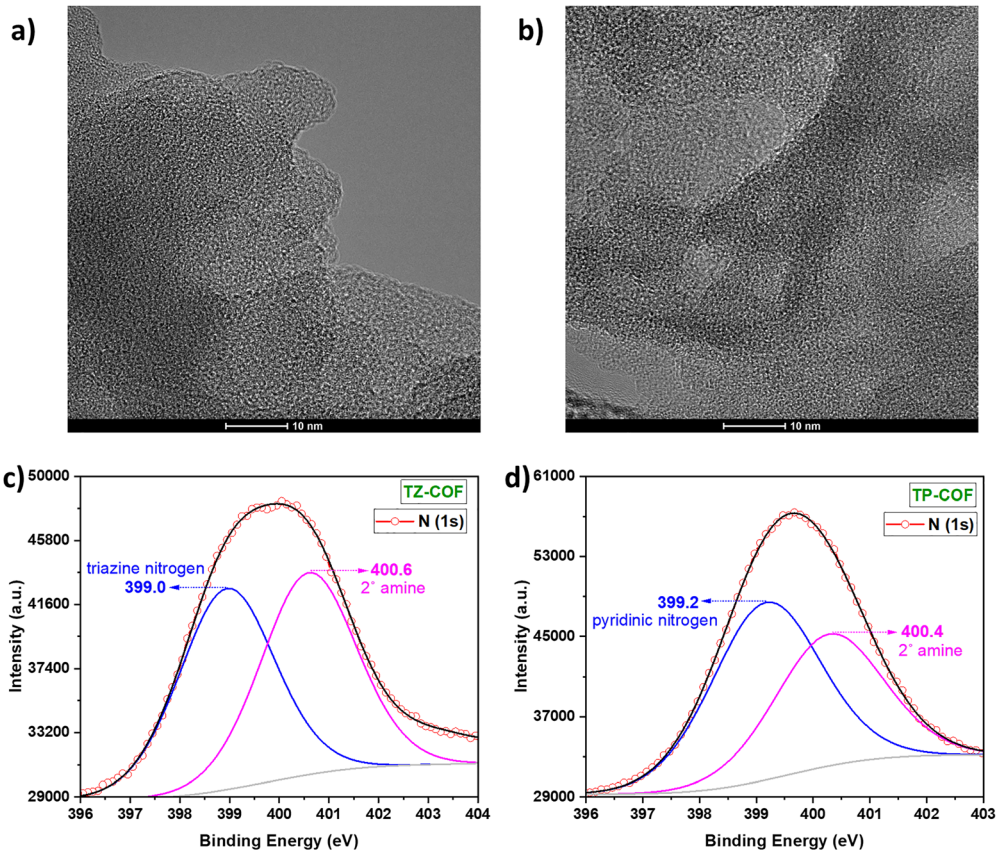

Fig. 2 TEM image of (a) TZ-COF and (b) TP-COF; N 1s XPS spectra of (c) TZ-COF and (d) TP-COF.

The higher proton conductivity of PA@TP-COF can be attributed to the synergistic interaction between phosphoric acid and the pyridinic nitrogen and oxygen atoms (keto group) within the COF skeleton. This interaction leads to a tightly bound phosphoric acid immobilized within the pore channels.[39] As a result, an increased number of proton carriers within the pore channels results in a surge in proton conductivity. To understand the high proton conduction in PA@TP-COF, the binding energy of phosphoric acid with the nitrogen and oxygen sites present on the single pore wall of PA@COFs was calculated using density functional theory (DFT) at the B3LYP/6-31G(d,p) level with the Gaussian 03 package (Fig. 4 and Table S4). For PA@TZ-COF, the calculated binding energy of phosphoric acid with triazine nitrogen is 5.72 kcal mol^{-1}, and for the carbonyl oxygen site it is −19.01 kcal mol^{-1}. In contrast, PA@TP-COF showed that the binding energy between phosphoric acid and pyridinic nitrogen/carbonyl oxygen sites is −20.09 kcal mol^{-1} (both values are identical). This higher binding energy revealed the strong ionic hydrogen bonding interaction between phosphoric acid and the pyridinic nitrogen/carbonyl oxygen sites in PA@TP-COF.[33] Additionally, the strong hydrogen bonding interaction results in tightly bound phosphoric acid within the pore. This affirms the synergistic interaction of phosphoric acid with pyridinic nitrogen and the carbonyl oxygen atom as depicted in Fig. 4b. Thus, phosphoric acid is confined within the pores, resulting in an enhanced proton conductivity. Conversely, the lower binding energy suggests feebly bound phosphoric acid with nitrogen/oxygen sites through weak hydrogen bonding in PA@TZ-COF, resulting in moderate proton conductivity.

In addition, we calculated the activation energy (E_a) for the proton conduction across the 1D channels of both COFs (Fig. 3b). The temperature-dependent proton conductivity $\sigma(T)$ can be described by the Arrhenius equation of $\sigma(T) = \sigma_0 e^{-E_a/RT}$, where σ_0 is the pre-exponential factor, E_a is the activation energy (eV), R is the universal gas constant (8.3144 J K^{-1} mol^{-1}), and T is the absolute temperature in K. From the $\ln \sigma$ *versus* temperature (T^{-1}), we calculated E_a to be 0.14 and 0.41 eV for PA@TZ-COF and PA@TP-COF, respectively (Fig. 3b). Since 0.41 eV is closer to 0.4 eV, proton conduction takes place *via* the Grotthuss mechanism of hopping of a hydrogen ion in both cases.[40]

Furthermore, the proton conductivity of PA@COFs under humidified conditions was also probed for their feasible conduction under mild temperature conditions (80 °C). Proton conductivity is raised under humidified conditions as compared to anhydrous conditions at 80 °C. As the humidity increased from 40 to 60, 80, and 95% relative humidity (RH), proton conductivity gradually increased (Fig. 3c and Fig. S15). The maximum proton conductivity of 2.2 × 10^{-4} S cm^{-1} was recorded for PA@TZ-COF at 80 °C and 95% RH. This value was slightly higher than that of PA@TZ-COF under anhydrous

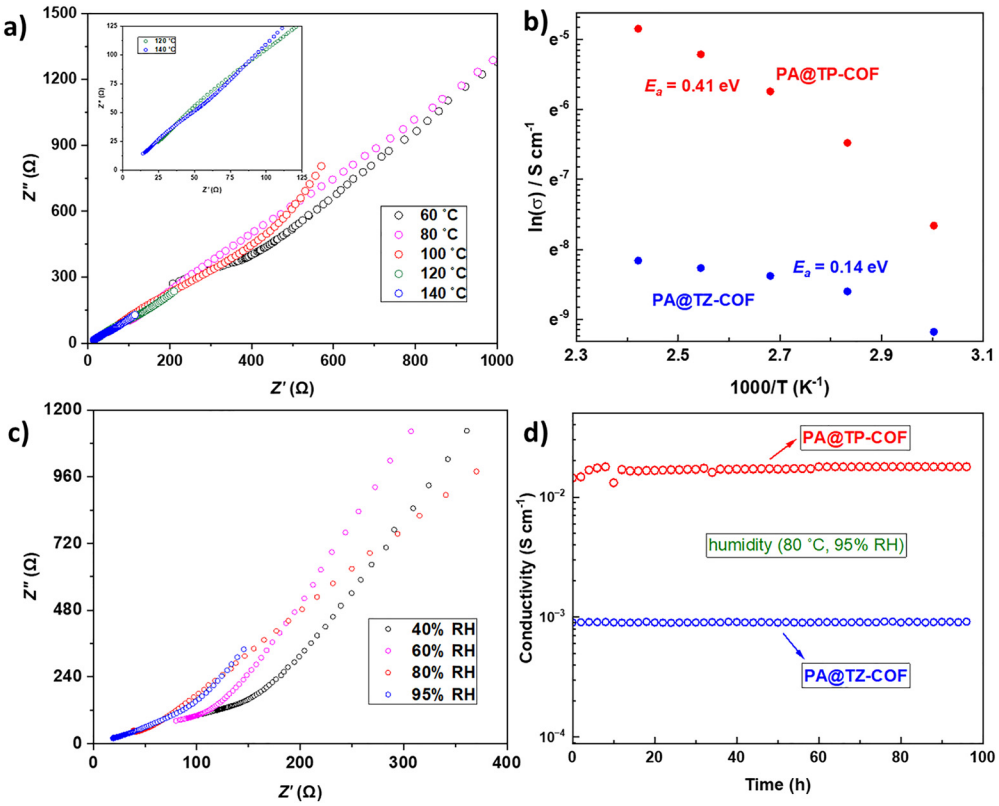

Fig. 3 (a) Nyquist plot for PA@TP-COF under anhydrous conditions. (b) Arrhenius plot for TZ-COF and TP-COF. (c) Nyquist plot for PA@TP-COF under humidified conditions at 80 °C. (d) Stability test carried out by measuring proton conductivity under humidified conditions (80 °C, 95% RH) at an interval of 2 h.

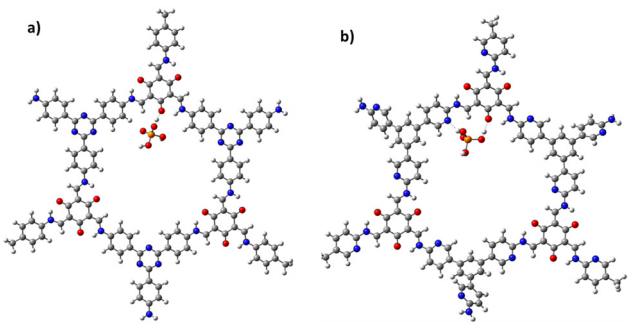

Fig. 4 DFT simulation model of one pore of (a) TZ-COF interacting with PA at the oxygen site and (b) TP-COF interacting with PA at both the oxygen and nitrogen sites (red: oxygen, blue: nitrogen, grey: carbon, white: hydrogen).

conditions. This might be due to the availability of a greater number of water molecules under humidified conditions, which increases proton conductivity. On the other hand, the proton conductivity of PA@TP-COF increased significantly as the humidity increased from 40 to 95% RH. The maximum proton conductivity of 1.2×10^{-2} S cm^{-1} was observed for PA@TP-COF at 80 °C and 95% RH. This could be attributed to accelerated water absorption in PA@TP-COF due to extended hydrogen bonding between pyridinic nitrogen, water and phosphoric acid, which favors the uninterrupted flow of protons.[32] Moreover, we investigated the stability of proton conduction under humidified conditions over 96 h at 2 h intervals (Fig. 3d and Fig. S16–S19). Though the proton conduction is steady for PA@TZ-COF, the magnitude of proton conduction falls short for practical applications. Interestingly, the proton conductivity of PA@TP-COF is steady and increases to 1.8×10^{-2} S cm^{-1} under continuous operation at 95% RH and 80 °C after 4 days (96 hours). This could be attributed to the stability of TP-COF after doping with PA, as well as the combined ionic hydrogen bonding interaction between water, PA, and pyridinic nitrogen and carbonyl oxygen, which leads to an uninterrupted flow of protons *via* the hopping mechanism.

4. Conclusions

In summary, we have successfully synthesized and characterized two COFs containing triazine and pyridine rings in their skeleton. Both COFs present high crystallinity, as evidenced by sharp PXRD peaks. The phosphoric acid-doped COF containing pyridinic nitrogen (PA@TP-COF) displayed maximum proton conductivity of 7.9×10^{-3} S cm^{-1} at 140 °C under anhydrous conditions, which is higher than that of PA@TZ-COF containing triazine nitrogen (2.9×10^{-4} S cm^{-1}). The high proton conductivity of TP-COF is attributed to the synergistic

interaction between phosphoric acid and carbonyl oxygen, as well as pyridinic nitrogen. This interaction leads to a strong ionic hydrogen bonding interaction and thus steady proton flow *via* proton hopping. Furthermore, the proton conductivity increases to 1.2 × 10^{-2} S cm^{-1} at 80 °C and 95% RH. Additionally, the excellent retention and augmented proton conductivity of PA@TP-COF under continuous exposure to humidified conditions for over 4 days indicates its potential for practical applications.

Author contributions

V. J.: conceptualization, data curation, methodology, formal analysis, and writing – original draft; K. M.: data curation, methodology, validation, formal analysis; H. A.: data curation, validation, formal analysis; M. J. P.: data curation, validation, formal analysis; K. Ł.: data curation, validation, formal analysis; A. N.: project administration, supervision, and writing – review and editing.

Conflicts of interest

The authors declare no competing financial interest.

Data availability

The data supporting this article have been included as part of the supplementary information (SI). Supplementary information is available. See DOI: **https://doi.org/10.1039/d5ma00722d**.

Acknowledgements

We are grateful for the ''ENSEMBLE3-Center of Excellence for nanophononics, advanced materials and novel crystal growth-based technologies'' project (GA No. MAB/2020/14) carried out under the International Research Agenda programs of the Foundation for Polish Science that are co-financed by the European Union under the European Regional Development Fund and the European Union Horizon 2020 research and innovation program Teaming for Excellence (GA. No. 857543) for partially supporting this work. The publication was created also as part of the project of the Minister of Science and Higher Education ''Support for the activities of Centers of Excellence established in Poland under the Horizon 2020 program'' under contract no. MEiN/2023/DIR/3797. We gratefully acknowledge Poland's high-performance computing infrastructure PLGrid (HPC Centers: ACK Cyfronet AGH) for providing computer facilities and support within computational grant no. PLG/2023/016865.

References

1 Q. Zhang, S. Dong, P. Shao, Y. Zhu, Z. Mu, D. Sheng, T. Zhang, X. Jiang, R. Shao, Z. Ren, J. Xie, X. Feng and B. Wang, Covalent organic framework–based porous ionomers for high-performance fuel cells, *Science*, 2022, **378**, 181–186, DOI: **10.1126/science.abm6304**.

2 S. Ahmad, T. Nawaz, A. Ali, M. F. Orhan, A. Samreen and A. M. Kannan, An Overview of Proton Exchange Membranes for Fuel Cells: Materials and Manufacturing, *Int. J. Hydrogen Energy*, 2022, **47**, 19086–19131, DOI: **10.1016/j.ijhydene.2022.04.099**.

3 S. Haldar, A. Schneemann and S. Kaskel, Covalent Organic Frameworks as Model Materials for Fundamental and Mechanistic Understanding of Organic Battery Design Principles, *J. Am. Chem. Soc.*, 2023, **145**, 13494–13513, DOI: **10.1021/jacs.3c01131**.

4 K. Jiao, J. Xuan, Q. Du, Z. Bao, B. Xie, B. Wang, Y. Zhao, L. Fan, H. Wang, Z. Hou, S. Huo, N. P. Brandon, Y. Yin and M. D. Guiver, Designing the Next Generation of Proton-Exchange Membrane Fuel Cells, *Nature*, 2021, **595**, 361–369, DOI: **10.1038/s41586-021-03482-7**.

5 K. A. Mauritz and R. B. Moore, State of Understanding of Nafion, *Chem. Rev.*, 2004, **104**, 4535–4586, DOI: **10.1021/cr0207123**.

6 A. Kusoglu and A. Z. Weber, New Insights into Perfluorinated Sulfonic-Acid Ionomers, *Chem. Rev.*, 2017, **117**, 987–1104, DOI: **10.1021/acs.chemrev.6b00159**.

7 A. Kraytsberg and Y. Ein-Eli, Review of Advanced Materials for Proton Exchange Membrane Fuel Cells, *Energy Fuels*, 2014, **28**, 7303–7330, DOI: **10.1021/ef501977k**.

8 A. P. Cote, A. I. Benin, N. W. Ockwig, M. O'Keeffe, A. J. Matzger and O. M. Yaghi, Porous, Crystalline, Covalent Organic Frameworks, *Science*, 2005, **310**, 1166–1170, DOI: **10.1126/science.1120411**.

9 C. S. Diercks and O. M. Yaghi, The Atom, The Molecule, and The Covalent Organic Framework, *Science*, 2017, **355**, eaal1585, DOI: **10.1126/science.aal1585**.

10 D. Zhu, J.-J. Zhang, X. Wu, Q. Yan, F. Liu, Y. Zhu, X. Gao, M. M. Rahman, B. I. Yakobson, P. M. Ajayan and R. Verduzco, Understanding Fragility and Engineering Activation Stability in Two-Dimensional Covalent Organic Frameworks, *Chem. Sci.*, 2022, **13**, 9655–9667, DOI: **10.1039/D2SC03489A**.

11 S. Kandambeth, A. Mallick, B. Lukose, M. V. Mane, T. Heine and R. Banerjee, Construction of Crystalline 2D Covalent Organic Frameworks with Remarkable Chemical (Acid/Base) Stability via a Combined Reversible and Irreversible Route, *J. Am. Chem. Soc.*, 2012, **134**, 19524–19527, DOI: **10.1021/ja308278w**.

12 A. Nagai, *Covalent Organic Frameworks*, Jenny Stanford Publishing, 2020.

13 K. Chang, H. Huang, Y. Meng, Z. Ju, H. Song, L. Zhang, X. Niu and Z.-J. Li, Synthesis of a Pyridine-Based Covalent Organic Framework as an Efficient Adsorbent for Rhodamine B Removal, *RSC Adv.*, 2023, **13**, 23682–23689, DOI: **10.1039/D3RA04184K**.

14 P. Rathi, S. Chowdhury, P. P. Das, A. K. Keshri, A. Chaudhary and P. F. Siril, Pore-Interface Engineering Improves Doxorubicin Loading to Triazine-Based Covalent Organic Framework, *Mater. Adv.*, 2024, **5**, 136–142, DOI: **10.1039/D3MA00673E**.

15 S. Chandra, T. Kundu, S. Kandambeth, R. BabaRao, Y. Marathe, S. M. Kunjir and R. Banerjee, Phosphoric Acid Loaded Azo (−N═N−) Based Covalent Organic Framework for Proton Conduction, *J. Am. Chem. Soc.*, 2014, **136**, 6570–6573, DOI: **10.1021/ja502212v**.

16 S. Haldar, R. Kushwaha, R. Maity and R. Vaidhyanathan, Pyridine-Rich Covalent Organic Frameworks as High-Performance Solid-State Supercapacitors, *ACS Mater. Lett.*, 2019, **1**, 490–497, DOI: **10.1021/acsmaterialslett.9b00222**.

17 Q. Cui, M. Zhou, Q. Wen, L. Li, C. Xiong, M. Adeli, L. Cheng, X. Xu, X. Ren and C. Cheng, Pyridine-Bridged Covalent Organic Frameworks with Adjustable Band Gaps as Intelligent Artificial Enzymes for Light-Augmented Biocatalytic Sensing, *Small*, 2024, **20**, 2401673, DOI: **10.1002/smll.202401673**.

18 A. Nagai, X. Chen, X. Feng, X. Ding, Z. Guo and D. Jiang, A Squaraine-Linked Mesoporous Covalent Organic Framework, *Angew. Chem. Int. Ed.*, 2013, **52**, 3770–3774, DOI: **10.1002/anie.201300256**.

19 R.-M. Zhu, J.-X. Fu, L.-H. Chen, J.-D. Feng and Z.-G. Gu, Covalent Organic Frameworks Confining Ultra-Dense Hydrated Hydrogen-Bond Networks for Efficient Intrinsic Proton Conduction, *Mater. Chem. Front.*, 2023, **7**, 5932–5940, DOI: **10.1039/D3QM00803G**.

20 Y. Zhang, C. Li, Z. Liu, Y. Yao, M. M. Hasan, Q. Liu, J. Wan, Z. Li, H. Li and Y. Nagao, Intrinsic Proton Conduction in 2D Sulfonated Covalent Organic Frameworks Through a Post-Synthetic Strategy, *CrystEngComm*, 2021, **23**, 6234–6238, DOI: **10.1039/D1CE00957E**.

21 Y. Yang, X. He, P. Zhang, Y. H. Andaloussi, H. Zhang, Z. Jiang, Y. Chen, S. Ma, P. Cheng and Z. Zhang, Combined Intrinsic and Extrinsic Proton Conduction in Robust Covalent Organic Frameworks for Hydrogen Fuel Cell Applications, *Angew. Chem. Int. Ed.*, 2020, **59**, 3678–3684, DOI: **10.1002/anie.201913802**.

22 S. Li, Y. Liu, L. Li, C. Liu, J. Li, S. Ashraf, P. Li and B. Wang, Enhanced Proton Conductivity of Imidazole-Doped Thiophene-Based Covalent Organic Frameworks via Subtle Hydrogen Bonding Modulation, *ACS Appl. Mater. Interfaces*, 2020, **12**, 22910–22916, DOI: **10.1021/acsami.0c04002**.

23 S. Chandra, T. Kundu, K. Dey, M. Addicoat, T. Heine and R. Banerjee, Interplaying Intrinsic and Extrinsic Proton Conductivities in Covalent Organic Frameworks, *Chem. Mater.*, 2016, **28**, 1489–1494, DOI: **10.1021/acs.chemmater.5b04947**.

24 S. Tao and D. Jiang, Accelerating Anhydrous Proton Transport in Covalent Organic Frameworks: Pore Chemistry and its Impacts, *Angew. Chem. Int. Ed.*, 2024, **63**, e202408296, DOI: **10.1002/anie.202408296**.

25 V. Joseph and A. Nagai, Recent Advancements of Covalent Organic Frameworks (COFs) as Proton Conductors Under Anhydrous Conditions for Fuel Cell Applications, *RSC Adv.*, 2023, **13**, 30401–30419, DOI: **10.1039/D3RA04855A**.

26 K. Maegawa, M. Wlazło, V. Joseph, K. Łyczko, Y. Korol, M. J. Potrzebowski, A. Matsuda and A. Nagai, Heteroatom-Embedded Mellitic Triimido COFs for Efficient Proton Conduction, *Sci. Rep.*, 2025, **15**, 5758, DOI: **10.1038/s41598-025-90291-x**.

27 V. Joseph, K. Maegawa, M. Wlazło, M. J. Potrzebowski, K. Łyczko and A. Nagai, Dual-Acid-Tailored Ionic Covalent Organic Frameworks for High-Temperature Proton Conduction under Anhydrous Conditions and the Practical Opportunities, *Chem. Mater.*, 2025, **37**, 2561–2568, DOI: **10.1021/acs.chemmater.5c00016**.

28 N. Agmon, The Grotthuss Mechanism, *Chem. Phys. Lett.*, 1995, **244**, 456–462, DOI: **10.1016/0009-2614(95)00905-J**.

29 K.-D. Kreuer, Proton Conductivity: Materials and Applications, *Chem. Mater.*, 1996, **8**, 610–641, DOI: **10.1021/cm950192a**.

30 K.-D. Kreuer, A. Rabenau and W. Weppner, Vehicle Mechanism, A New Model for the Interpretation of the Conductivity of Fast Proton Conductors, *Angew. Chem. Int. Ed.*, 1982, **21**, 208–209, DOI: **10.1002/anie.198202082**.

31 B. Shi, X. Pang, S. Li, H. Wu, J. Shen, X. Wang, C. Fan, L. Cao, T. Zhu, M. Qiu, Z. Yin, Y. Kong, Y. Liu, M. Zhang, Y. Liu, F. Pan and Z. Jiang, Short Hydrogen-Bond Network Confined on COF Surfaces Enables Ultrahigh Proton Conductivity, *Nat. Commun.*, 2022, **13**, 6666, DOI: **10.1038/s41467-022-33868-8**.

32 X. Yang, Y. Fu, M. Liu, S. Zheng, X. Li, Q. Xu and G. Zeng, Solvent Effects on Metal-Free Covalent Organic Frameworks in Oxygen Reduction Reaction, *Angew. Chem. Int. Ed.*, 2024, **63**, e202319247, DOI: **10.1002/anie.202319247**.

33 G. Jiang, W. Zou, Z. Ou, L. Zhang, W. Zhang, X. Wang, H. Song, Z. Cui, Z. Liang and L. Du, Tuning the Interlayer Interactions of 2D Covalent Organic Frameworks Enables an Ultrastable Platform for Anhydrous Proton Transport, *Angew. Chem. Int. Ed.*, 2022, **61**, e202208086, DOI: **10.1002/anie.202208086**.

34 S. Zhang, L. Lombardo, M. Tsujimoto, Z. Fan, E. K. Berdichevsky, Y.-S. Wei, K. Kageyama, Y. Nishiyama and S. Horike, Synthesizing Interpenetrated Triazine-based Covalent Organic Frameworks from CO_2, *Angew. Chem. Int. Ed.*, 2023, **62**, e202312095, DOI: **10.1002/anie.202312095**.

35 S. Jiang, H. Niu, X. Gu and Y. Cai, Perfluoroalkyl Functionalized Superhydrophobic Covalent Organic Frameworks for Excellent Oil–Water Membrane Separation and Anhydrous Proton Conduction, *Small*, 2024, **20**, 2403772, DOI: **10.1002/smll.202403772**.

36 W. Zhang, J. Ji, H. Li, J. Li, Y. Sun, Y. Tang, T. Yang, W. Jin, Y. Zhao, C. Huang and C. Gong, Nitrogen-Rich Covalent Organic Frameworks Composited High-Temperature Proton Exchange Membranes with Ultralow Volume Expansion and Reduced Phosphoric Acid Leakage, *ACS Appl. Mater. Interfaces*, 2024, **16**, 52309–52325, DOI: **10.1021/acsami.4c10408**.

37 L. Liu, L. Yin, D. Cheng, S. Zhao, H.-Y. Zang, N. Zhang and G. Zhu, Surface-Mediated Construction of an Ultrathin Free-Standing Covalent Organic Framework Membrane for Efficient Proton Conduction, *Angew. Chem. Int. Ed.*, 2021, **60**, 14875–14880, DOI: **10.1002/anie.202104106**.

38 L. Wang, Y. Wang, Z. Li, T. Li, R. Zhang, J. Li, B. Liu, Z. Lv, W. Cai, S. Sun, W. Hu, Y. Lu and G. Zhu, PAF-6 Doped with Phosphoric Acid through Alkaline Nitrogen Atoms Boosting

High-Temperature Proton-Exchange Membranes for High Performance of Fuel Cells, *Adv. Mater.*, 2023, **35**, 2303535, DOI: **10.1002/adma.202303535**.

39 S. Sharma, K. Maegawa, H. Alipour, Y. Korol, M. Potrzebowski and A. Nagai, Phosphoric Acid-Merged Squaraine Conjugated Mesoporous Polymer with High Proton Conductivity, *Chem. Commun.*, 2025, **61**, 9087–9090, DOI: **10.1039/d5cc01294e**.

40 D. I. Kolokolov, D.-W. Lim and H. Kitagawa, Characterization of Proton Dynamics for the Understanding of Conduction Mechanism in Proton Conductive Metal-Organic Frameworks, *Chem. Rec.*, 2020, **20**, 1297–1313, DOI: **10.1002/tcr.202000072**.